



Trans. Nonferrous Met. Soc. China 27(2017) 2181-2192

Transactions of Nonferrous Metals Society of China

www.tnmsc.cn



Electrochemical corrosion behaviour of stir zone of friction stir welded dissimilar joints of AA6061 aluminium–AZ31B magnesium alloys

R. KAMAL JAYARAJ, S. MALARVIZHI, V. BALASUBRAMANIAN

Centre for Materials Joining and Research (CEMAJOR), Department of Manufacturing Engineering, Annamalai University, Annamalai Nagar 608002, Tamil Nadu, India

Received 6 August 2016; accepted 23 December 2016

Abstract: Joining of dissimilar metals will offer many advantages in transportation sectors such as fuel consumption, weight reduction and emission reduction. However, joining of aluminium (Al) alloys with magnesium (Mg) alloys by fusion welding process is very complicated. Friction stir welding (FSW) is a feasible method to join these two dissimilar alloys. Mixing these two metals together in stir zone (SZ) leads to poor corrosion resistance. In this investigation, an attempt has been made to understand the corrosion resistance of SZ of FSWed dissimilar joints of AA6061 Al alloy and AZ31B Mg alloy. Potentiodynamic polarization test was conducted by varying chloride ion concentration, pH value of the NaCl solution and exposure time. The corroded surfaces were analyzed using optical microscopy, scanning electron microscopy and XRD techniques. Of these three factors investigated, exposure time is found to be the most significant factor to influence the corrosion behaviour of SZ of friction stir welded dissimilar joints of Al/Mg alloys.

Key words: friction stir welding; aluminium alloy; magnesium alloy; dissimilar joint; corrosion behaviour

1 Introduction

In recent times, much attention has been shifted towards dissimilar joints, especially in automotive industries; aluminium (Al)/magnesium (Mg) dissimilar joints are to be used in automobiles to reduce the mass of the vehicles. But joining of these alloys by fusion welding techniques is very difficult task due to differences in crystal structures [1]. The formation of intermetallic compounds is also a major problem in dissimilar joints, which leads to extremely brittle joints [2]. In order to reduce volume fraction of the intermetallic compounds, low heat processes are required. Under these circumstances, friction stir welding (FSW) and variants of FSW process can be used to join the dissimilar alloys [3-5]. FSW joints exhibit different zones like stir zone (SZ), thermomechanically affected zone (TMAZ) and heat affected zone (HAZ). Due to the presence of inhomogeneous structure across the welded cross-section of FSW joint, it is necessary to study the corrosion behaviour of the FSW joint. ALIREZA et al [6] reported that the intercalated microstructure could be observed in the stir zone due to mixing of two metals

during welding. This complex flow pattern present in the stir zone creates galvanic coupling due to differences in potential between the two metals. Therefore, it is more vital to study the corrosion behaviour of stir zone of the dissimilar FSW joints.

LIU et al [7] studied the galvanic corrosion behaviour of dissimilar friction stir welded joint made of AZ31 magnesium alloy and AA2024 aluminum alloy. They reported that the predominant locations of the corrosion attack were observed in the narrow regions of Mg alloy adjacent to Al alloy areas, where there was a low ratio of anode-to-cathode surface area. The corrosion was mainly due to the establishment of a strong galvanic couple between Al and Mg alloys in the dissimilar FSWed joints. ESTHER et al [8] studied the influence of friction stir welding process parameters on dissimilar joints between Al alloy and pure copper alloy. They revealed that corrosion resistance of the welds was improved as the rotational speed was increased. DONATUS et al [9] investigated the corrosion susceptibility of dissimilar friction stir welds of AA5083-O and AA6082-T6 alloys. They revealed that the faster welding speed resulted in increased susceptibility to corrosion because of the reduced tool

rotational rate per weld length for generating heat and mixing of materials. In addition, they reported that, grain boundary sensitization in the HAZ of both alloys, distribution of Mg_2Si particles along the boundary between the two alloys and the galvanic contacts between the AA5083-rich zones and the AA6082-rich zones were responsible for the corrosion susceptibility in the welds.

From the literature review, it is understood that the published information on the effect of corrosion test parameters (chloride ion concentration, pH of the solution and exposure time) on corrosion behaviour of friction stir welded aluminium and magnesium dissimilar joints is very scant. Hence, the present investigation was carried out to study the effect of pH, chloride ion concentration and exposure time on corrosion resistance of stir zone of friction stir welded dissimilar joints of AA6061 Al and AZ31B Mg alloys.

2 Experimental

Rolled plates of AZ31B Mg alloy and AA6061-T6 Al alloy plates with 6 mm in thickness were used as base materials in this study. The chemical compositions of these alloys are presented in Table 1. To fabricate FSW joint, the plates were sliced to the required size (150 mm × 75 mm) by power hacksaw. A square butt joint was obtained by securing the plates in position using mechanical clamps. The welding direction was normal to the rolling direction of the plates. Figure 1(a) shows the positioning of the plates during welding, where AA6061 Al alloy was placed on the advancing side and AZ31B Mg alloy on retreating side. Taper threaded cylindrical tool made of super high speed steel (Fig. 1(b)) was used to fabricate the joints.

Table 1 Chemical composition of AA6061 Al and AZ31B Mg alloys (mass fraction, %)

Alloy	Al	Zn	Si	Mn	Cu	Cr	Mg
AA6061	Bal.	-	0.6	-	0.25	0.2	1.0
AZ31B	3.0	1.0	0.1	0.6	0.04	_	Bal.

A computer numerical controlled (CNC) friction stir welding machine (22 kW, 4000 r/min, 60 kN) was used to fabricate the joints. From Ref. [10], the optimized welding parameters and tool dimensions were taken to

fabricate the joints. The specimens were extracted from weld nugget region of the FSW joints for conducting potentiodynamic polarization test with the dimensions of 20 mm × 20 mm × 6 mm. The scheme of extraction of corrosion test samples is shown in Fig. 1(c). Before corrosion test, the specimens were ground and polished with 600- to 1500-grit SiC paper. Finally, it was cleaned with acetone and rinsed in distilled water and then dried by warm flowing air. The photograph of the polished corrosion test specimen is shown in Fig. 1(d). The sample placed in a corrosion test cell is shown in Fig. 1(e). The Gill-AC potentiostat instrument was used to conduct the potentiodynamic polarization test in NaCl solution under different conditions as shown in Fig. 1(f).

A central composite rotatable three-factor, five-level factorial design matrix was chosen to minimize number of experimental conditions.

The experimental design matrix consisting of 20 sets of coded conditions, comprising a full replication three-factor factorial design of eight points, six star points, and six center points was used. Table 2 presents the range of factors considered and the lower and upper limits of the parameters were coded as -1.68 and +1.68, respectively. NaCl solutions with concentrations of 0.2, 0.36, 0.6, 0.84 and 1 mol/L were prepared. The pH value of the solution was measured using a digital pH meter and varied from 3 to 11 as prescribed by design matrix.

The microstructural examination in the stir zone was carried out before and after corrosion test using a light optical microscope. Corroded surfaces were analyzed by scanning electron microscope (SEM). XRD analysis was carried out to characterize the corrosion products formed on the surface of the specimen. The optical micrographs of parent metals and stir zone of dissimilar friction stir welded joint are shown in Fig. 2.

3 Development of empirical relationship

3.1 Corrosion rate evaluation

The polarization tests were carried out in corrosion cell containing 500 mL of NaCl solution. The electrochemical cell consists of stir zone as the working electrode, saturated calomel as reference electrode and platinum as counter electrode. The specimens were exposed in the NaCl solution, and a polarization scan was carried out towards more noble values at a rate of $1\,\text{mV/s}$.

Table 2 Important factors and their levels

Series	Series Factor	Notation	Unit -			Level		
No.				-1.68	-1	0	+1	+1.68
1	Chloride ion concentration	С	mol/L	0.2	0.36	0.6	0.84	1
2	pH value	P		3	4.62	7	9.38	11
3	Exposure time	t	min	5	15	30	45	55

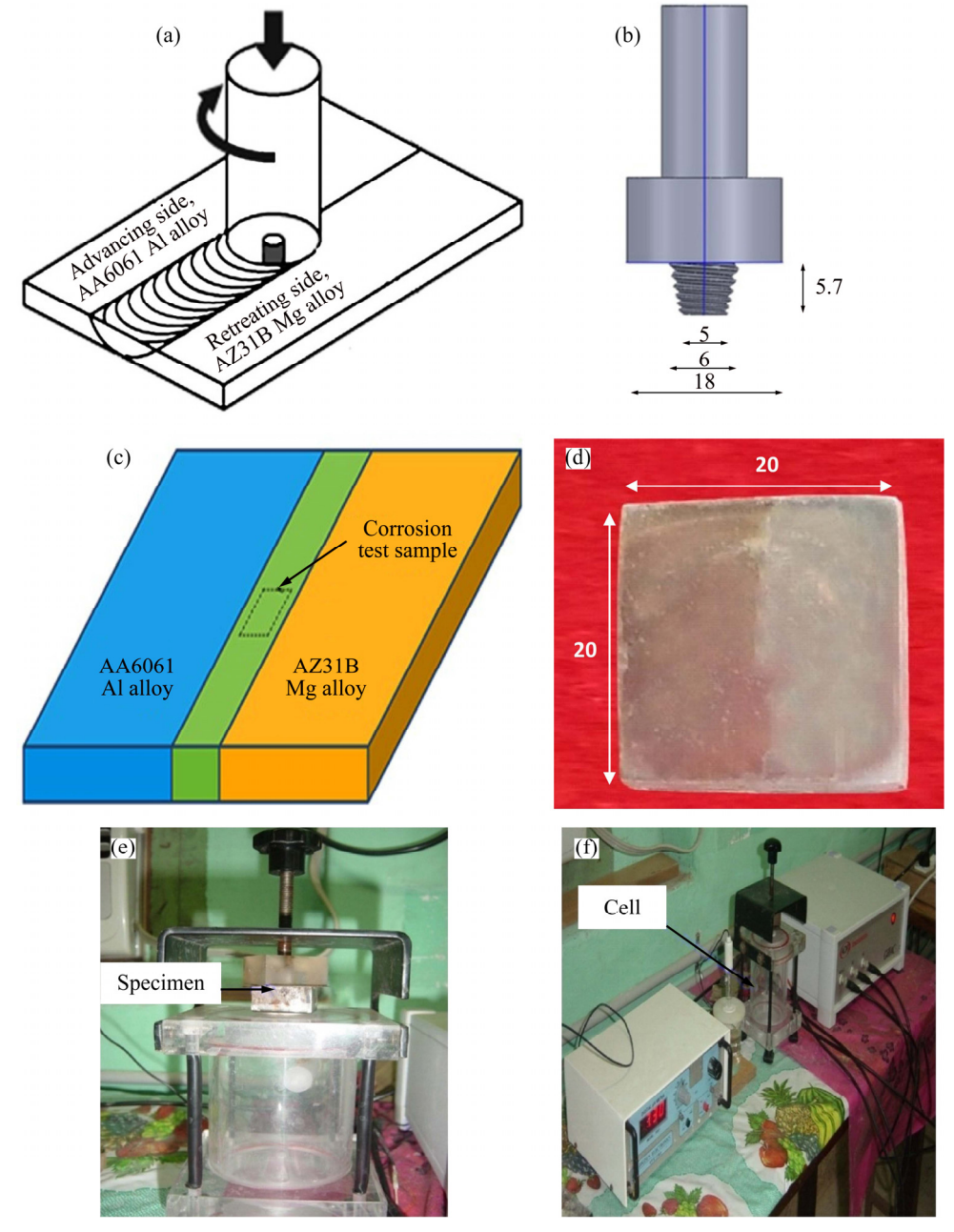


Fig. 1 Experimental details (unit: mm): (a) FSW of dissimilar joint (Schematic diagram); (b) Tool dimensions; (c) Specimen extraction scheme; (d) Dimensions of corrosion test specimen; (e) Corrosion test cell; (f) Gill AC potentiostat

The corrosion rate η in mm/a (mm/year) of the weld nugget region was calculated using the following expression:

$$\eta = (J_{\text{corr}}F)/1000$$
 (1)

The current density J_{corr} in A/m² was calculated using following expression:

$$J_{\text{corr}} = (b_{\text{a}}b_{\text{c}})/[2.3R_{\text{p}}(b_{\text{a}}+b_{\text{c}})]$$
 (2)

where b_a is anodic Tafel slope in V, b_c is the cathodic Tafel slope in V, and R_p is the polarization resistance in Ω/m^2 .

The metal factor F was calculated using the following expression:

$$F = tK/\rho \tag{3}$$

where t is the seconds in a year (a), ρ is the density in g/cm^3 and K is the electrochemical equivalent in g/C. Thus, the evaluated corrosion rates of the experiments are presented in Table 3.

3.2 Empirical relationship to predict corrosion rate

A second order quadratic model was developed to correlate the electrochemical corrosion test parameters. The response (corrosion rate) is a function of chloride ion concentration (c), pH value (P), and exposure time (t).

$$\eta = f\{c, P, t\} \tag{4}$$

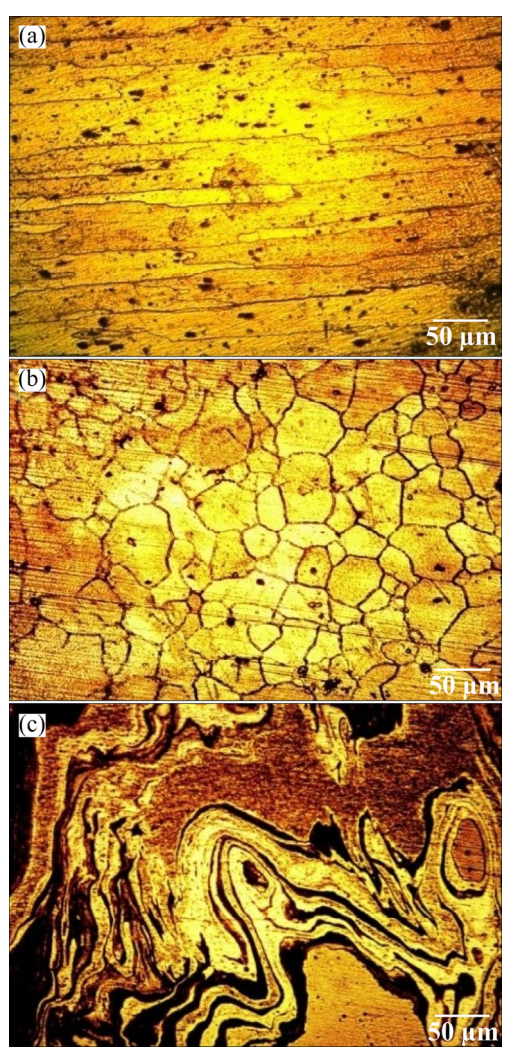


Fig. 2 Optical micrographs of AA6061 Al alloy (a), AZ31B Mg alloy (b) and weld nugget region of friction stir welded dissimilar joints (c)

The equation should contain main and interaction effects of all variables and hence the response is expressed as

$$Y = b_0 + \sum b_i x_i + \sum b_{ii} x_i^2 + \sum b_{ij} x_i x_j$$
 (5)

For three factors, the selected response could be expressed as

$$\eta = b_0 + b_1 c + b_2 P + b_3 t + b_{12} c P + b_{13} c t + b_{23} P t + b_{33} t^2 \tag{6}$$

where b_0 is the average of responses (corrosion rate) and b_1 , b_2 , b_3 , \cdots , b_{11} , b_{12} , b_{13} , \cdots , b_{22} , b_{23} , b_{33} are the coefficients that depend on their respective main and interaction factors, which were calculated using the expression given below:

$$B_i = \sum_i (X_i, Y_i) / n \tag{7}$$

where i varies from 1 to n, X_i is the corresponding coded value of a factor and Y_i is the corresponding response

Table 3 Design matrix and experimental results

Expt. No.	$c(\text{Cl}^-)/$ $(\text{mol}\cdot\text{L}^{-1})$	рН	Exposure time/min	$\eta/$ (mm·a ⁻¹)	
1	0.36	4.62	15	27.99	
2	0.84	4.62	15	35.43	
3	0.36	9.38	15	21.51	
4	0.84	9.38	15	25.99	
5	0.36	4.62	45	18.89	
6	0.84	4.62	45	23.98	
7	0.36	9.38	45	15.08	
8	0.84	9.38	45	18.68	
9	0.20	7.00	30	18.47	
10	1.00	7.00	30	28.12	
11	0.60	3.00	30	28.60	
12	0.60	11.00	30	18.03	
13	0.60	7.00	5	30.84	
14	0.60	7.00	55	16.20	
15	0.60	7.00	30	23.02	
16	0.60	7.00	30	23.09	
17	0.60	7.00	30	23.18	
18	0.60	7.00	30	22.92	
19	0.60	7.00	30	23.21	
20	0.60	7.00	30	22.68	

output value (corrosion rate) attained from the experiment and n is the total number of combination considered. All the coefficients were calculated by applying central composite face centred design using the Design Expert statistical software package. Analysis of variance (ANOVA) test was used to find out the significant coefficients and the results are presented in Table 4. From the ANOVA test results, the squared terms c^2 and P^2 are found to be insignificant at 95% confidence level. The final relationship was developed by incorporating significant coefficients only.

The final empirical relationship derived by the above method to estimate the corrosion rate (in mm/a) of nugget region (stir zone) of friction stir welded Al/Mg dissimilar joint is given below:

$$\eta = -53.03 + 122.12c + 10.81P + 0.42t - 0.48cP - 0.07ct - 0.02Pt - 0.007t^{2}$$
(8)

4 Results and discussion

4.1 Effect of pH on corrosion rate

To understand the effect of pH, the chloride ion concentration and exposure time were kept constant at 0.6 mol/L and 30 min, respectively, whereas the pH level was varied from 3 to 11. Figure 3(a) shows the effect of

Table 4 ANOVA test results

Source	Sum of square	Df	Mean square	F value	<i>p</i> -value Prob> <i>F</i>	
Model	497.99	9	55.33	720.59	< 0.0001	Significant
c	99.37	1	99.37	1294.15	< 0.0001	
P	134.17	1	134.17	1747.35	< 0.0001	
t	254.13	1	254.13	3309.48	< 0.0001	
cP	2.48	1	2.48	32.24	0.0002	
ct	1.30	1	1.30	16.98	0.0021	
Pt	5.80	1	5.80	75.49	< 0.0001	
c^2	0.17	1	0.17	2.19	0.1700	
P^2	0.19	1	0.19	2.48	0.1462	
t^2	0.51	1	0.51	6.60	0.0280	
Residual	0.77	10	0.077			
Lack of fit	0.58	5	0.12	3.00	0.1268	Not significant
Pure error	0.19	5	0.038			
Cor total	498.76	19				

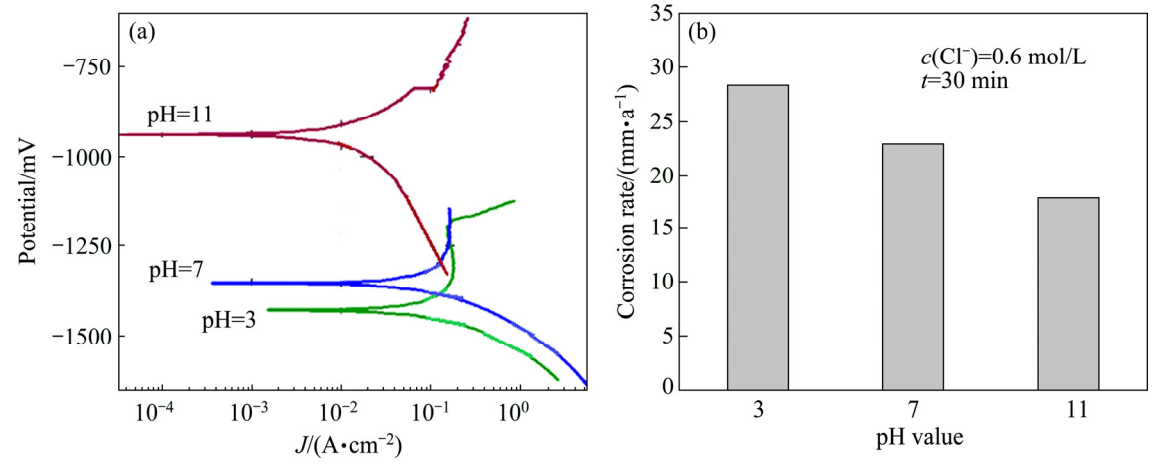


Fig. 3 Effect of pH value of NaCl solution on potentiodynamic polarization curves (a) and corrosion rate (b)

pH on potentiodynamic polarization curves. It can be seen that at pH 3, the anodic curve of the materials showed a shift to higher current density and at pH 11, the anodic curve shifted to low current density. The aluminium and magnesium φ -pH diagram predicted that there should be no film on a magnesium surface in a solution with a pH lower than 11 because Al(OH)₃ and Mg(OH)₂ are not stable under such conditions. However, even though it is not thermodynamically stable at low pH values, the dissolution kinetics may be slower and a surface film may be formed if the dissolution kinetics is slower than the formation kinetics. It was observed that the corrosion rate usually increased with the decrease in the pH value of the solutions [11]. The dissolution of aluminium and magnesium in aqueous solutions proceeds by the reduction of oxygen to produce aluminium and magnesium hydroxide. The reduction process is mainly water reduction, thus forming Al(OH)₃ and Mg(OH)₂ protective layer. The higher pH value

favors the formation of Al(OH)₃ and Mg(OH)₂, which protects the alloy from corrosion.

Figure 3(b) shows the effect of pH of NaCl solution on corrosion rate of stir zone of friction stir welded dissimilar joints of Al/Mg alloys. The results demonstrate that, the pH value has an inversely proportional relationship with the corrosion rate, i.e., when the pH level increases, the corrosion rate decreases [12]. The highest corrosion rate was observed in pH 3 solution and the lowest corrosion rate was observed in pH 11 solution.

The surface of the specimen is composed of aluminium and magnesium alloys, when it is exposed to lower pH solution the solubility of Al³⁺ facilitates the dissolution of the Al matrix and further accelerates the chloride attack. The dissolution of Mg in aqueous solutions proceeded by the reduction of water to produce Mg hydroxide Mg(OH)₂ and hydrogen gas (H₂). However, the mechanism of corrosion of the Al matrix in

neutral and alkaline media is related with the formation of protective layer of aluminum hydroxides Al(OH)3. The oxide film is uniformly thinned by the chemical dissolution, which is facilitated by the presence of high OH concentration in alkaline solution [13]. Whereas in neutral pH solutions, the passive film of Al(OH)3 formed on AA6061 Al alloy surface is remarkably stable due to its low solubility, which acts as protector for this alloy against corrosive agents. In addition, it was seen that, the specimen surfaces were severely corroded at all pH values and higher chloride concentrations. The corrosion of AZ31B alloy was significantly influenced by pH value. The equilibrium pH value required for the precipitation of Mg(OH)2 is around 11. Highly acidic solutions are aggressive towards Mg, hence there is a very high corrosion rate. It was seen that more corrosion products appeared in lower pH than higher pH solutions. The corrosion rate and consequently the rate and extent of hydrogen evolution were found to increase significantly with decreasing the pH of solution. At lower pH values, a rise in corrosion rate exhibited with the increase in chloride ion concentration. The corrosion rates obtained from the lower and higher concentrations of solution with constant pH value and exposure time of 7 and 30 min were found to be 5.4798 and 14.1368 mm/a, respectively. But the quantity of this rise was different in such a way that, the change in chloride ion concentration at lower concentrations affected the corrosion rate much more as compared to that of higher concentrations. This showed that with the increase in chloride ion concentration, the rising rate of corrosion rate decreased, that is, the influence of chloride ion concentration was much lower at higher concentrations [14].

During the electrolysis reaction, water was actually splitting into hydrogen and oxygen molecules. When the current is applied to the electrolysis unit, the electrons on the cathode end will combine with water, causing each water molecule to release one hydrogen atom. These hydrogen atoms are combined to form hydrogen bubbles and leave negatively charged ions of hydroxyl group (OH⁻).

The following anodic and cathodic reactions take place in NaCl environments:

$$Mg \rightarrow Mg^{2+} + 2e$$
 (Anodic reaction) (9)

$$2H_2O+2e \rightarrow H_2+2OH^-$$
 (Cathodic reaction) (10)

Firstly, Mg dissolves and Mg²⁺ cations are produced according to Eq. (9), possibly through intermediate steps involving divalent Mg²⁺. Secondly, Mg dissolution is accompanied by hydrogen evolution according to Eq. (10), since Mg in neutral and low pH aqueous solutions is well below the region of water stability. Finally, pH rises along with the cathodic reaction due to

the formation of OH⁻, which favours the formation of Mg(OH)₂. Thus, the overall reaction could be expressed as

$$Mg^{2+}+2OH^{-} \longrightarrow Mg(OH)_2$$
 (Corrosion product) (11)

Therefore, as the pH of the solution decreases the corrosion kinetics and the hydrogen evolution reaction proceed at much faster rate.

The passive film (Al₂O₃) forms from reaction of aluminium with oxygen and aqueous solutions. It forms according to the following reaction:

$$4Al+3O_2 \longrightarrow 2Al_2O_3 \tag{12}$$

$$2Al+3H_2O \rightarrow Al_2O_3+6H^++6e$$
 (13)

Aluminium and its alloys have shown good resistance to corrosion in neutral solutions, atmospheric environment and some acidic solutions, due to the formation of a protective oxide film on their surfaces. The formed oxide film has a low rate of dissolution in aqueous solutions of pH 7. However, it dissolves in pH solutions of 3 and 11.

The corrosion process of aluminium in the presence of aggressive solutions is an electrochemical process which involves dissolution of aluminium.

The oxide film dissolves in both acidic and high alkalinity solutions according to the following reactions:

$$Al_2O_3+6H^+ \longrightarrow 2Al^{3+}+3H_2O$$
 (Acidic solution) (14)
 $Al_2O_3+3H_2O+2OH^- \longrightarrow 2Al(OH)_4^-$ (Alkaline solution)

On the contrary, in neutral solutions, the oxide film is stable and functions as a barrier between the aluminium substrate and the surrounding environment. Thus, it inhibits passage of electrons and protects the aluminium substrate from the attack of aggressive solutions.

The optical micrograph and scanning electron micrograph of the corroded specimens are shown in Figs. 4(a) and (b), respectively. On the surface of the specimen exposed to NaCl solution, magnesium coupled with aluminium alloy which sacrificed its ability and corrode severely, revealing that at lower pH values, surface of the AZ31B Mg alloy was completely corroded, corrosion attack was almost distributed on the entire surface. Visible corrosion attack was observed when the pH value increased. In pH 3 solution, the hydrogen bubbles overflowed and broke away from the surface of the specimens.

From Figs. 4(a) and (b), it was found that at higher pH values, corrosion has been observed only at the edges of the surface and also several tiny corrosion attacks created on the surface of the AZ31B Mg alloy. Nevertheless it still suffered much less corrosive attack when compared to lower pH values.

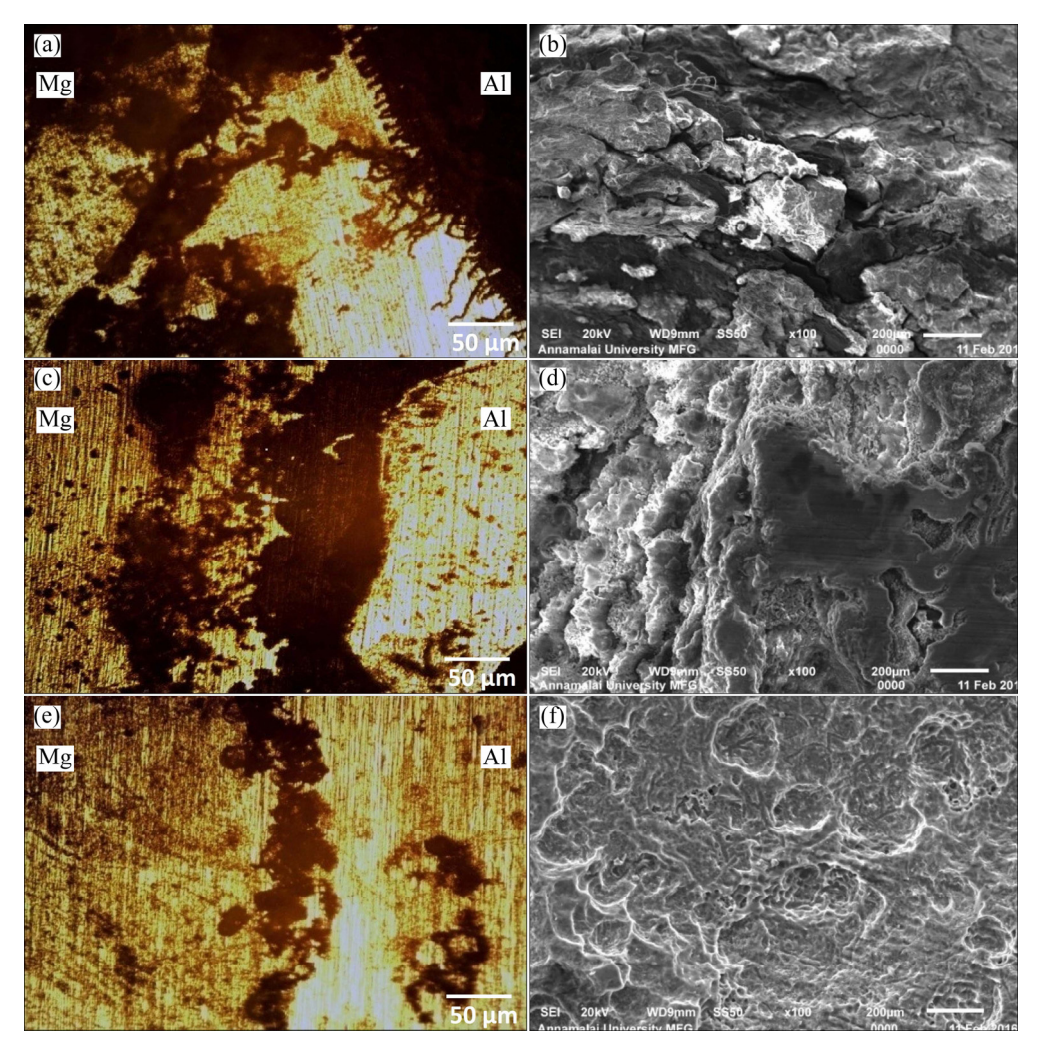


Fig. 4 Effect of pH on corrosion morphology of stir zone: (a) OM, pH=3; (b) SEM, pH=3; (c) OM, pH=7; (d) SEM, pH=7; (e) OM, pH=11; (f) SEM, pH=11

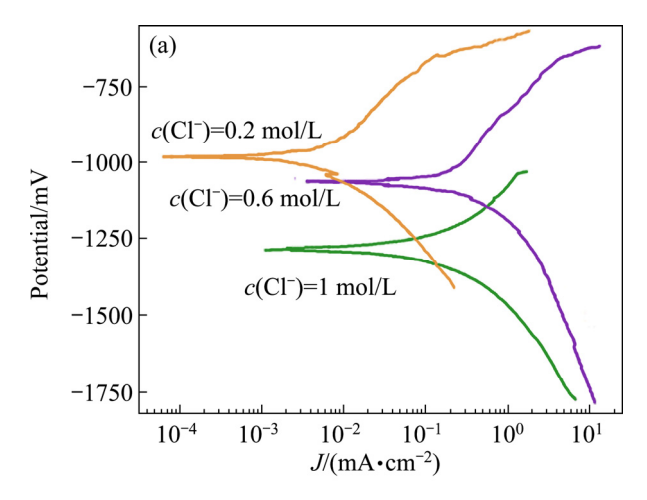
4.2 Effect of chloride ion concentration on corrosion rate

In order to study the effect of chloride ion concentration, the pH and exposure time were kept constant at 7 and 30 min, respectively while the chloride ion varied from 0.2 to 1.0 mol/L. Figure 5(a) shows the effect of chloride ion concentration on potentiodynamic polarization curve. From Fig. 5(a), it can be seen that with the increase of chloride ion concentration in the solutions, the anodic curve of the materials showed a shift to higher current density values, which may be explained by the adsorption of chloride ion on the alloy surface at weak parts of oxide film. The adsorption of chloride ions to oxide-covered magnesium surface transformed Mg(OH)₂ to easily soluble MgCl₂. Thus, the corrosion rate became severe due to penetration of hydroxide film by chloride ions [15]. Also, weak parts of oxide film may occur due to intermetallics present in FSZ of AA6061–AZ31B alloys. The weak parts of oxide film may occur due to intermetallics such as Al₁₂Mg₁₇.

These intermetallics are the initiation sites for corrosion in AA6061-AZ31B alloys.

Figure 5(b) shows the effect of Cl⁻ concentration on corrosion behavior of dissimilar FSWed SZ of AA6061–AZ31B alloys in NaCl solution. It is seen that the alloy exhibited a rise in corrosion rate with the increase in Cl⁻ concentration and thus the change of Cl⁻ concentration affected the corrosion rate much more in higher concentration solutions than that in lower concentration solutions.

It was also observed that, the surface corrosion region increased in ratio, with the increase of chloride ion concentration. Normally, chloride ions are very aggressive to magnesium compared to aluminium, so that the corrosion regions are more on magnesium side in SZ of AA6061–AZ31B alloys. The increase in corrosion rate with increasing chloride ion concentration was attributed to the participation of chloride ions in the dissolution reaction. When the AA6061–AZ31B alloys get in touch with NaCl solution which is exposed



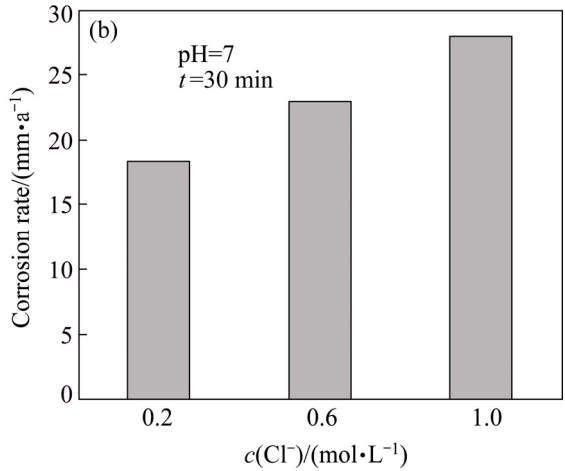


Fig. 5 Effect of chloride ion concentration on potentiodynamic polarization curves (a) and corrosion rate (b)

to atmosphere, the following electrochemical reaction occurs, as shown in Eq. (16). The anodic reaction is

$$M \rightarrow M^+ + e$$
 (16)

where M=Al and Mg; M⁺=Al³⁺ and Mg²⁺.

Since the medium is exposed to the atmosphere, it contains dissolved oxygen. So, the cathodic reaction is in the form given in Eq. (17).

$$O_2 + 2H_2O + 4e \longrightarrow 4OH^- \tag{17}$$

Charge conservation is maintained in both the metal and solution. Every electron produced during the formation of metal ion is immediately consumed by the oxygen reduction reaction. Also, one hydroxyl ion is produced for every metal ion in the solution. This process is self-stimulating and self-propagating. After a short interval, the oxygen on the corroded surface is depleted because of restricted convection, so oxygen reduction ceases in this area. After oxygen is depleted, no further oxygen reduction occurs, although the rapid dissolution of metal (M) on the corroded surface tends to produce excess of positive charge (M⁺) in exposed area, which is necessarily balanced by the migration of

chloride ions to maintain electroneutrality. Thus, on the corroded surface there is a high concentration of MCl and as a result of hydrolysis, high concentration hydrogen ions are produced and shown in Eq. (18):

$$MCl+H2O \rightarrow MOH \downarrow +H^{+}+Cl^{-}$$
 (18)

Both hydrogen and chloride ions stimulate the dissolution of most metals and alloys, and the entire process accelerates with time. Since the solubility of oxygen is virtually zero in concentrated solutions, no oxygen occurs on the corroded surface. The cathodic oxygen reduction on the surface adjacent to corroded surface tends to suppress corrosion. Thus, the chloride ion stimulates metal dissolution, and this change tends to produce conditions that are favorable to further rapid dissolution at one particular point [16]. Also, because of the presence of intermetallics which act as a site for crack growth in the stir zone the rate of metal dissolution is momentarily high at this point [17].

Figure 6 shows influence of chloride concentration on the corrosion morphology of the specimen exposed in pH 7 of NaCl solution for 30 min with different chloride ion concentrations of 0.2, 0.6 and 1 mol/L. Here, it is observed that the corrosion obtained from potentiodynamic polarization tests is quite variable in size with the difference in chloride ion concentration of the solution. At higher chloride ion concentration $(c(C1^-)=1 \text{ mol/L})$, the corrosion attack becomes widen and deep. Also at lower chloride ion concentration $(c(Cl^{-})=0.2 \text{ mol/L})$, the corrosion attack seems to be small and forms on the limited surface only. It is also exposed that at higher chloride ion concentration, the surface of the AA6061-AZ31B alloys is completely corroded, corrosion attack almost distributes on the entire surface compared to 0.6 mol/L Cl⁻, and also the diameter of the corroded surface increases with the increase in chloride ion concentration. The increasing trend of the corroded surface area with the increase of chloride ion concentration is attributed to the attack of Cl on the surface, leading to converting Mg(OH)₂ film into MgCl₂. The same thing occurs on aluminium side but chloride ions are very insistent to magnesium compared to aluminium. However, with the decrease of chloride ion concentration, the ions become less aggressive, hence, the formation of corrosion attack is very low as evidenced by the corroded surface examination (Fig. 6).

Figures 6(a) and (b) reveal that at lower chloride ion concentrations, less corrosion attacks are formed on the surface of the AZ31B Mg alloy. The chloride ion concentration increases, some obvious corrosion attacks appear on the surface of the specimen.

4.3 Effect of exposure time on corrosion rate

In order to examine the effect of exposure time, the pH value and chloride ion concentration were kept constant at 7 and 0.6 mol/L, respectively, while the exposure time varied from 5 to 55 min. Figure 7(a) shows the influence of exposure time on potentio-dynamic polarization curve for the AA6061–AZ31B alloys, obtained in a solution of 0.6 mol/L NaCl at neutral pH with different exposure time of 5, 30, and 55

min. It can be seen that the anodic curve of the materials shows a shift to higher current density values and corrosion potential shifts to more negative (active) values with the decrease in exposure time and the corrosion current density decreases with increasing exposure time. This is suggested the existence of the corrosion film of NaCl solution with the increase of exposure time.

During the initiation of corrosion process in acidic solution, the evolution of hydrogen bubbles on the alloy

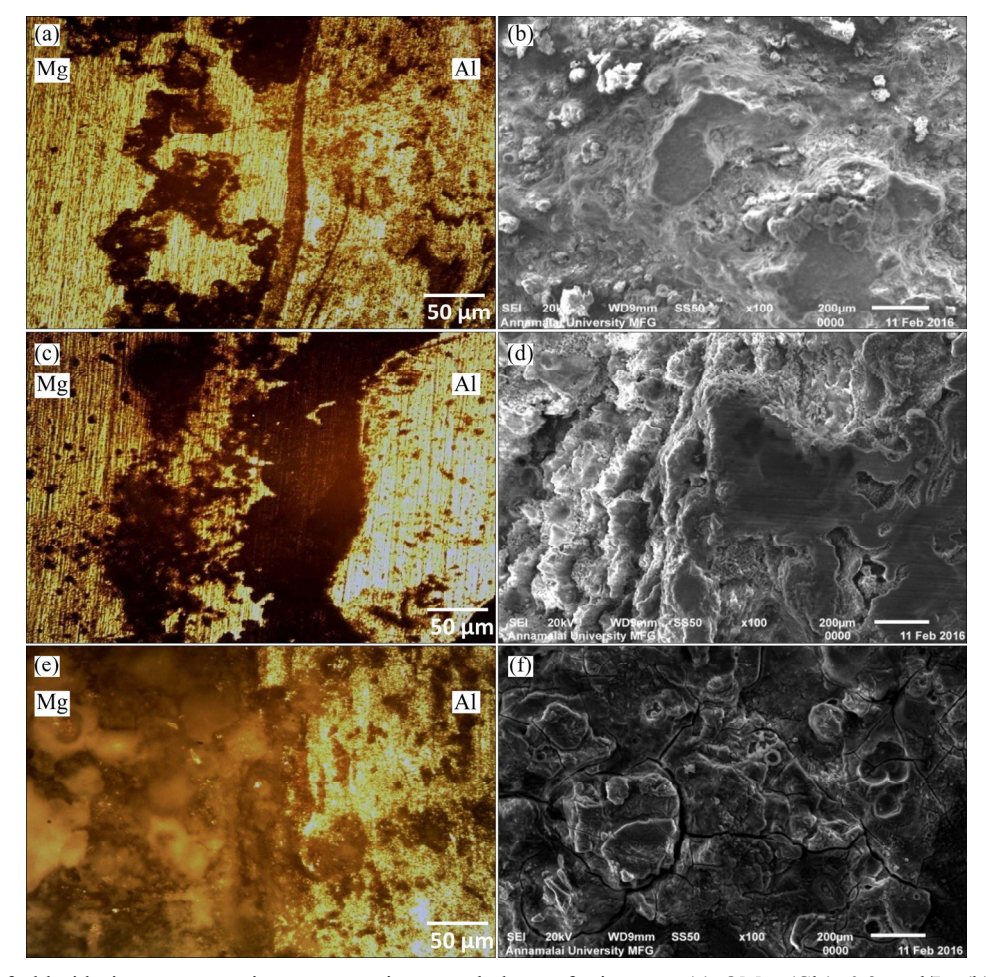


Fig. 6 Effect of chloride ion concentration on corrosion morphology of stir zone: (a) OM, $c(C\Gamma)=0.2 \text{ mol/L}$; (b) SEM, $c(C\Gamma)=0.2 \text{ mol/L}$; (c) OM, $c(C\Gamma)=0.6 \text{ mol/L}$; (d) SEM, $c(C\Gamma)=0.6 \text{ mol/L}$; (e) OM, $c(C\Gamma)=1 \text{ mol/L}$; (f) SEM, $c(C\Gamma)=1 \text{ mol/L}$

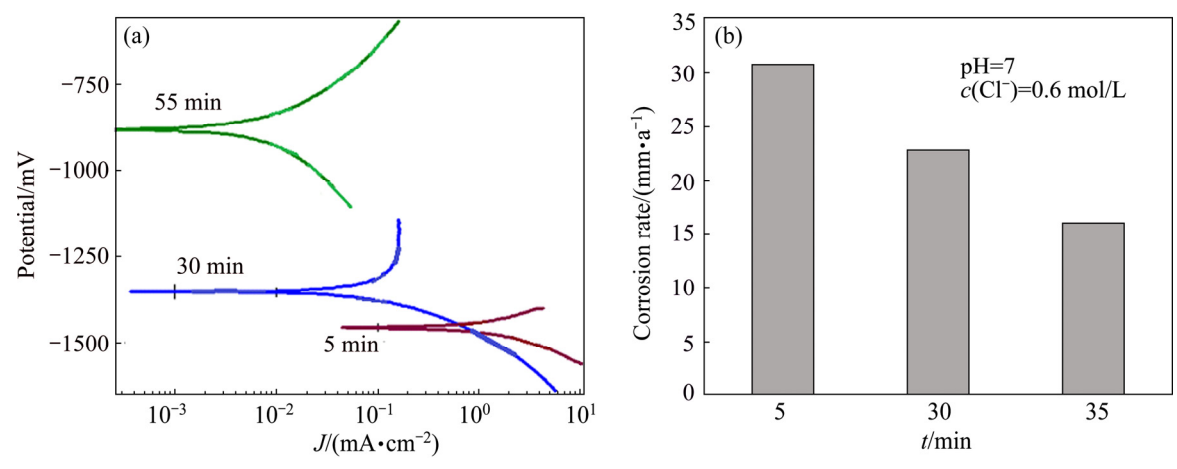


Fig. 7 Effect of exposure time on potentiodynamic polarization curves (a) and corrosion rate (b)

surface transiently increased the corrosion rate through removal of the corrosion product film, meanwhile, hydrogen bubbles also reduced corrosion rate in the period of the growth and absorption through shielding of the surface. With the increase of exposure time, hydrogen reacted with Al-Mg and there were protective MgH₂ and AlH₂ films formed on alloy surface. Hence, the corrosion rate of AA6061-AZ31B alloys decreased evidently with the increase in exposure time. In the same way in alkaline solution, aluminium and magnesium hydroxide films were formed during reduction reaction but Al(OH)₃ and Mg(OH)₂ films can be destroyed by Cl⁻ in the solution, the dissolution of the film resulted in aluminium and magnesium alloys to exposure to the solution, providing the active centre for further electrochemical reactions. Thus, the localized corrosion takes place on the surface. But after some exposure time the formation of the insoluble corrosion products may further retard the migration of ions on the surface of the specimen, thus reducing the electrochemical corrosion rate. That is, with increasing exposure time, the corrosion rate decreased. Thus, the corrosion rate decreased with an increase in exposure time, which implied that the initial corrosion product impeded the passage of corrosion medium and provided protection for metal substrates [18].

Figure 7(b) depicts the influence of the exposure time on the corrosion rate of AA6061–AZ31B alloys. From the bar graph, it can be inferred that the exposure time has an inversely proportional relationship with the corrosion rate. The corrosion rate decreased with the increase in time. This resulted from the decrease in hydrogen evolution with an increase in exposure time. This is attributed to the corrosion occurring over an increasing fraction of the surface, which is the insoluble corrosion product. The insoluble corrosion product on the surface of the alloy could slow down the corrosion rate [19].

Figures 8(a) and (b) show the effect of exposure time on the corrosion morphology of the specimen exposed in NaCl solution of pH 7 and chloride ion concentration of 0.6 mol/L with different exposure time

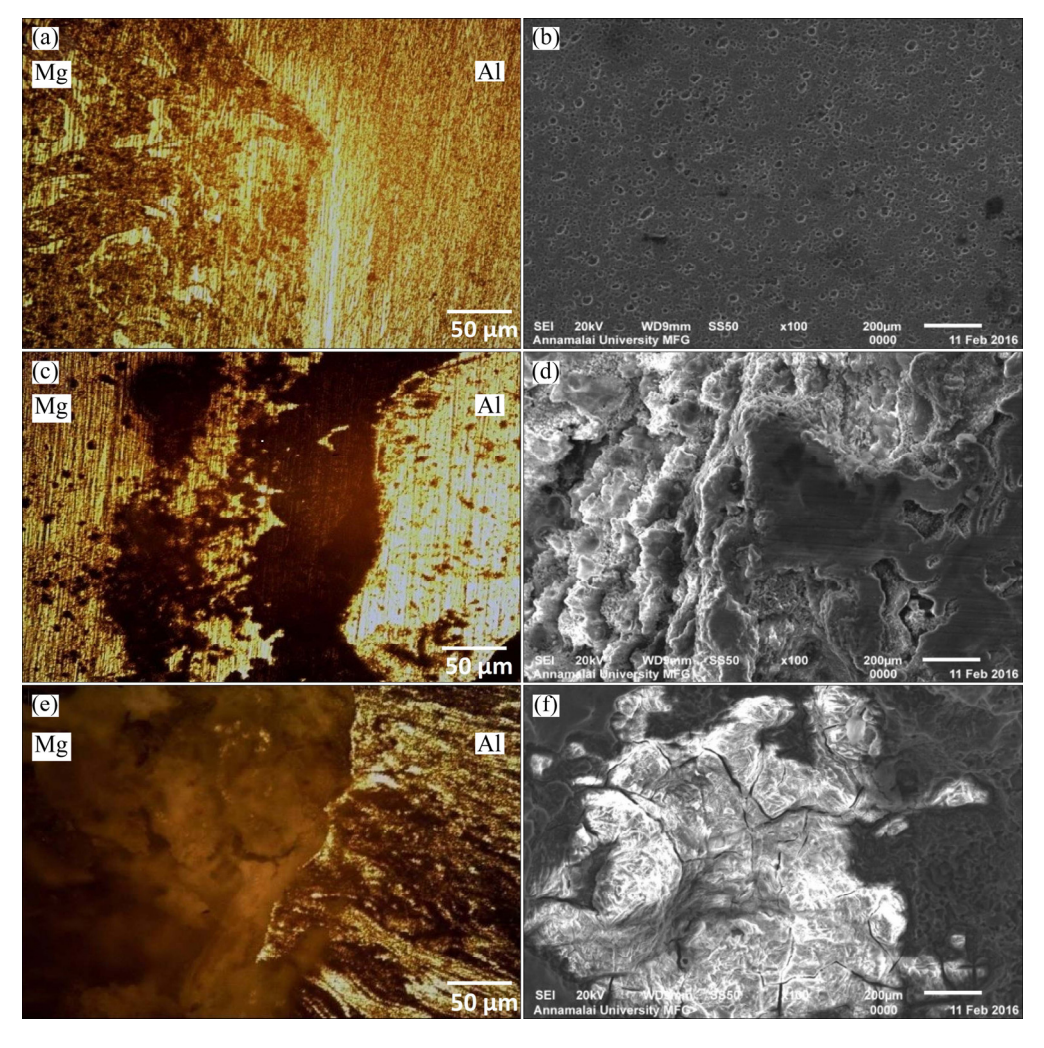


Fig. 8 Effect of exposure time on corrosion morphology of stir zone: (a) OM, t=5 min; (b) SEM, t=5 min; (c) OM, t=30 min; (d) SEM, t=30 min; (e) OM, t=55 min; (f) SEM, t=55 min

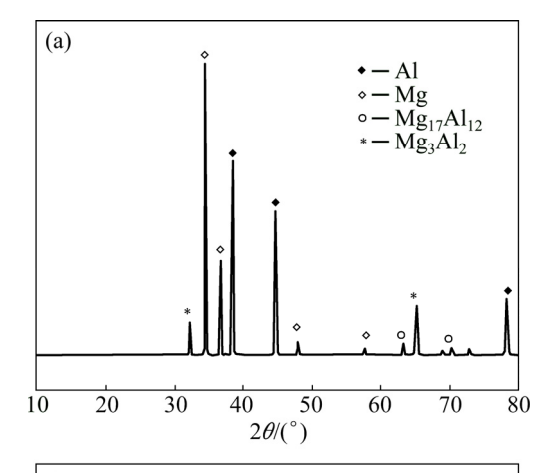
of 5, 30 and 55 min. Here, the corrosion obtained from potentiodynamic polarization tests varies with the difference in exposure time. At lower exposure time, the corrosion attack deepens but at higher exposure time, the corrosion attack seems to be little widened possessing corroded products in large size [20]. At the higher exposure time, a small amount of corrosion attack was observed on the surface of the material in wider state.

It is found that the size of the corrosion attack is deeper and more vigorous at 5 min because here hydrogen evolution is more compared with 30 and 55 min. But, at 30 and 55 min the rate of corrosion attack is reduced. The reason for decreasing corrosion rate with increasing exposure time is the decrease in hydrogen evolution. This is attributed to the corrosion occurring over an increasing fraction of the surface with the increase in time, which is the insoluble corrosion product. The insoluble corrosion product on the surface of the alloy could slow down the corrosion rate. Also, it is viewed from line scan that that hydrogen evolution is very hostile to magnesium compared to aluminium at 5 min, so the corrosion region is more in magnesium in friction stir zone of AA6061-AZ31B alloys. Also, at 5 min, the oxygen composition is low compared with 30 and 55 min, so the corrosion resistance on the metal surface adjacent to corroded surface is less at 5 min, which leads to the fact that the face of AA6061-AZ31B alloys is completely decayed. Moreover, the chloride is more at 5 min, this also tends to increase the size of the corrosion attack.

Figure 9(a) shows the XRD pattern for dissimilar joints of Al/Mg alloys, which exhibits Al, Mg matrix phases, confirming the presence of intermetallics Mg₁₇Al₁₂ and Al₃Mg₂ in the weld nugget. XRD patterns of the corrosion layer produced after corrosion test in NaCl solution reveal that Al(OH)₃ and Mg(OH)₂ are the main corrosion products as seen in Fig. 9(b).

5 Conclusions

- 1) An empirical relationship was developed to predict corrosion rate of stir zone of friction stir welded AA6061 Al and AZ31B Mg alloy dissimilar joints incorporating corrosion test parameters.
- 2) From the ANOVA test results, it is found that exposure time has more predominant effect on corrosion rate followed by pH value and chloride ion concentration of NaCl solution.
- 3) This research work illustrates that the corrosion rate of stir zone of friction stir welded dissimilar joints of Al/Mg alloy was higher in the acidic media than in alkaline and neutral media.
- 4) There is no passive film on magnesium and aluminium alloy surfaces in a solution with pH less than



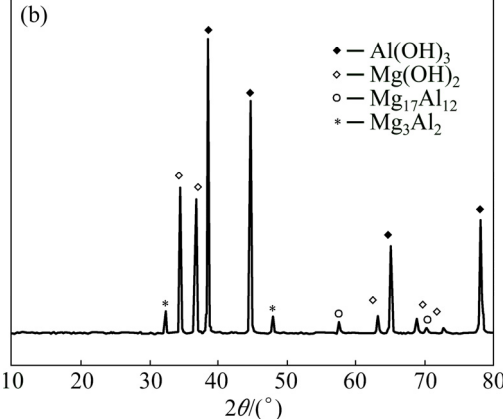


Fig. 9 XRD patterns of stir zone before (a) and after (b) corrosion test

or equal to 7 because $Mg(OH)_2$ is not stable under such conditions. The higher pH value favors the formation of $Mg(OH)_2$ which protects the alloy from corroding.

- 5) The chloride ions are more vigorous on the dissimilar welds (stir zone) of AA6061-AZ31B alloys and hence the increase in the chloride ion concentration enhances the corrosion rate.
- 6) The corrosion rate decreases with an increase in exposure time, which implies that the initial corrosion product impedes the passage of corrosion medium and provides protection for metal substrates.

Acknowledgements

The authors wish to express their sincere thanks to Council of Scientific and Industrial Research (CSIR), New Delhi, India, for the financial support to carry out this investigation through sponsored project No. 22(0615)/13/EMR-II dated 26.02.2013.

References

 LEE W B, YEON Y M, JUNE S B. The mechanical properties related to the dominant microstructure in the weld zone of dissimilar formed Al joints by friction stir welding [J]. Journal of Materials Science, 2003, 38: 4183–4191.

- [2] TAIKI M, ATSUSHI K, MASATO T, MAKOTO H, TOMOTAKE H, KENJI H. Dissimilar welding of Al and Mg alloys by FSW [J]. Materials Transactions, 2008, 49(5): 1129–1131.
- [3] MCLEAN A A, POWELL G L F, BROWN I H, LINTON V M. Friction stir welding of magnesium alloy AZ31B to aluminum alloy 5083 [J]. Science and Technology of Welding and Joining, 2003, 28: 462-464
- [4] LI Y, WEI Z, WANG Z, LI Y. Friction self-piercing riveting of aluminum alloy AA6061-T6 to magnesium alloy AZ31B [J]. Journal of Manufacturing Science and Engineering, 2013, 135: 0610071-0610077.
- [5] MA Y, LI Y, HU W, LOU M, LIN Z. Modeling of friction self-piercing riveting of aluminum to magnesium [J]. Journal of Manufacturing Science and Engineering, 2016, 138: 0610071-0610079.
- [6] ALIREZA M, ARVIN T, ATEFEH S, FARIBORZ S, JAMSHID A M. Microstructure and mechanical properties of friction stir weld of dissimilar AZ31-O magnesium alloy to 6061-T6 aluminum alloy [J]. Transactions of Nonferrous Metals Society of China, 2014, 24: 1317–1322.
- [7] LIU C, CHEN D, BHOLE S, CAO X, JAHAZI M. Polishing-assisted galvanic corrosion in the dissimilar friction stir welded joint of AZ31 magnesium alloy to 2024 aluminum alloy [J]. Materials Characterization, 2009, 60: 370–376.
- [8] ESTHER A T, ANTHONY A, STEPHEN A A. Effects of processing parameters on corrosion properties of dissimilar friction stir welds of aluminium and copper [J]. Transactions of Nonferrous Metals Society of China, 2014, 24: 1323–1330.
- [9] DONATUS U, THOMPSON G E, ZHOU X, WANG J, CASSELL A, BEAMISH K. Corrosion susceptibility of dissimilar friction stir welds of AA5083 and AA6082 alloys [J]. Materials Characterization, 2015, 107: 85–97.
- [10] MALARVIZHI S, BALASUBRAMANIAN V. Influences of tool shoulder diameter to plate thickness ratio (D/T) on stir zone formation and tensile properties of friction stir welded dissimilar joints of AA6061 aluminum–AZ31B magnesium alloys [J]. Materials and Design, 2012, 40: 453–460.
- [11] NOBUYOSHI H, YASUHIRO K, DAISUKE K, NOBURU A.

- Formation and break down of surface films on magnesium and its alloys in aqueous solutions [J]. Corrosion Science, 2007, 49: 166–175.
- [12] DHANAPAL A, RAJENDRA BOOPATHY S, BALA-SUBRAMANIAN V. Influence of pH value, chloride ion concentration and immersion time on corrosion rate of friction stir welded AZ61A magnesium alloy weldments [J]. Journal of Alloys and Compounds, 2012, 523: 49–60.
- [13] BROWN O R, WHITLEY J S. Electrochemical behaviour of aluminium in aqueous caustic solutions [J]. Electrochimica Acta, 1987, 32: 545–556.
- [14] THIRUMALAIKUMARASAMY D, SHANMUGAM K, BALA-SUBRAMANIAN V. Comparison of the corrosion behaviour of AZ31B magnesium alloy under immersion test and potentiodynamic polarization test in NaCl solution [J]. Journal of Magnesium and Alloys, 2014, 2: 36–49.
- [15] BLAWERT C, MORALES E D, DIETZEL W, KAINER K U. Comparison of corrosion properties of squeeze cast and thixocast Mg-Zn-RE alloys [J]. Materials Science Forum, 2005, 488: 697-700.
- [16] MARS FONTANA G. Corrosion engineering [M]. 3rd ed. New York: Tata McGraw Hill Education, 2005.
- [17] BALA SRINIVASAN P, ARORA K S, DIETZEL W, PANDEY S, SCHAPER M K. Characterisation of microstructure, mechanical properties and corrosion behaviour of an AA2219 friction stir weldment [J]. Journal of Alloys and Compounds, 2010, 492: 631–637
- [18] GHADA ABADY M, NADIA HILLAL H, MOHAMMED R, NAHZED BADARY A. Effect of Al content on the corrosion behavior of Mg-Al alloys in aqueous solutions of different pH [J]. Electrochimica Acta, 2010, 55: 6651-6658.
- [19] SONG Ying-wei, SHAN Da-yong, CHEN Rong-shi, HAN En-hou. Effect of second phases on the corrosion behavior of wrought Mg-Zn-Y-Zr alloy [J]. Corrosion Science, 2010, 52: 1830–1837.
- [20] ZHAO M C, SCHMUTZ P, BRUNNER S, LIU M, SONG G L, ATRENS A. An exploratory study of the corrosion of Mg alloys during interrupted salt spray testing [J]. Corrosion Science, 2009, 51: 1277-1292.

搅拌摩擦焊接 AA6061-AZ31B 合金异质接头 在搅拌区的电化学腐蚀行为

R. KAMAL JAYARAJ, S. MALARVIZHI, V. BALASUBRAMANIAN

Centre for Materials Joining and Research (CEMAJOR), Department of Manufacturing Engineering, Annamalai University, Annamalai Nagar 608002, Tamil Nadu, India

摘 要: 异质金属的连接在交通运输领域如燃料消耗降低、材料质量减轻、排放量减少等方面具有较多优越性。然而,采用熔焊工艺对铝、镁合金进行焊接是一个非常复杂的过程。搅拌摩擦焊接方法是一种对铝、镁合金进行连接的有效方法。在搅拌摩擦焊接过程中,铝、镁合金在搅拌区混合,致使合金在该区的耐蚀性能变差。本文作者研究搅拌摩擦焊 AA6061-AZ31B 合金异质接头的耐蚀性能,通过改变氯离子浓度、NaCl 溶液的 pH 值和焊接时间对样品进行恒电位极化实验。采用光学显微镜、扫描电镜和 X 射线衍射技术对样品的腐蚀表面进行表征。结果表明,在所研究的 3 个参数中,焊接时间对搅拌摩擦焊 AA6061-AZ31B 合金异质接头耐蚀性能的影响最显著。关键词: 搅拌摩擦焊; 铝合金; 镁合金; 异质接头; 腐蚀行为